Nucleated Crystallization of Isotactic Polypropylene in Multilayered Sandwich Nanocomposites with Gold Particles

Miroslav Slouf,[1] Antonin Sikora,[1] Ewa Pavlova,[1] Helena Vlkova,[1] Josef Baldrian,[1] Tomas Base,[2] Ewa Piorkowska[3]

[1]*Department of Morphology and Rheology of Polymer Materials, Institute of Macromolecular Chemistry, Academy of Sciences of the Czech Republic, 16206 Praha 6, Czech Republic*
[2]*Department of Synthesis, Institute of Inorganic Chemistry, Academy of Sciences of the Czech Republic, 250 68 Husinec-Řez 1001, Czech Republic*
[3]*Department of Polymer Structure, Centre of Molecular and Macromolecular Studies, Polish Academy of Sciences, Sienkiewicza 112, 90363 Lodz, Poland*

Received 30 November 2011; accepted 1 December 2011
DOI 10.1002/app.36589
Published online in Wiley Online Library (wileyonlinelibrary.com).

ABSTRACT: Nucleation of isotactic polypropylene (PP) crystallization by gold particles with various sizes and shapes was studied. The morphology of gold particles ranged from microcrystals with well-developed crystal facets (AuMC) to vacuum-sputtered 5 nm gold nanoparticles (AuNP), 30 nm gold nanoislands (AuNI), and compact gold nanolayer (AuNL). To minimize agglomeration of Au particles in molten PP, the nucleated crystallization was studied by means of the improved sandwich method, which consisted in the controlled deposition of a homogeneous nucleant layer between ~ 100 μm PP films, followed by the careful thermal treatment and the evaluation of the nucleation activity by three independent methods: polarized-light microscopy, two-dimensional wide-angle X-ray scattering, and differential scanning calorimetry. It was demonstrated that the nucleating activity of gold strongly depended on its morphology: The nucleation effect of microcrystalline AuMC resulted in a transcrystallization comparable to that caused by a strong commercial α-nucleant (Hyperform HPN-68), whereas the effect of vacuum-sputtered layers of nanocrystalline AuNL, AuNI, and AuNP was extremely weak. © 2012 Wiley Periodicals, Inc. J Appl Polym Sci 000: 000–000, 2012

Key words: isotactic poly(propylene); nucleated crystallization; gold nanoparticles; nanolayers; nanocomposites

INTRODUCTION

Polypropylene (PP) belongs among the five most used commodity polymers (low- and high-density polyethylene, PP, polystyrene, polyvinylchloride; Ref. 1). Its most widely used stereoisomer, isotactic polypropylene (iPP), is a semicrystalline, tough, flexible, and economical material.[2] End-use properties of PP can be further modified by controlled changes of its crystalline structure, which can be influenced by numerous organic and inorganic compounds, known as nucleating agents or nucleants.[3] Majority of the nucleating agents induce crystallization of the most frequent crystal polymorph, the α-phase[4]; fewer compounds induce the metastable polymorph with enhanced impact strength and toughness, the β-phase.[4,5]

The heterogeneous nucleation of polymer crystallization consists in overcoming an energy barrier, which is associated with formation of a critical nucleus. Classic nucleation theories attribute the heterogeneous nucleation to the lowering of an energy barrier due to the reduction the surface free energy of the crystals.[6] Numerous studies also demonstrated that epitaxial growth of crystals on the nucleants could be involved.[3,4] In any case, an efficient heterogeneous nucleation requires large surface of the nucleation agent, which multiplies the number of nucleation sites. For given amount, the nucleation agent surface can be enlarged by good dispersion of the nucleant in the polymer matrix and/or by decreasing nucleant particle size. Although decreasing particle size is beneficial for crystallization, it is evident that there must be a certain limit, below which the nucleant particles are too small to facilitate formation of critical nuclei on their surface.

Recent studies reported only weak or medium nucleating activity of ZnO, Al_2O_3 SiO_2, and Ag nanoparticles in PP.[7–10] In our own work, we showed that ~ 5 nm chemically synthesized Au

Correspondence to: M. Slouf (slouf@imc.cas.cz).
Contract grant sponsor: Grant Agency of the Czech Republic; contract grant number: P205/10/0348.
Contract grant sponsor: Academy of Sciences of the Czech Republic; contract grant number: KAN200520704.
Contract grant sponsor: Czech-Polish Academies of Sciences Bilateral Agreement.

nanoparticles[11] nucleated PP crystallization quite intensively even at very low concentrations starting from 0.001 wt %.[12] Simultaneously, we developed a sandwich method for reproducible study of microparticle and nanoparticle-induced nucleation effects, by means of which we managed to prove that the nucleating activity of ~ 5 nm vacuum-sputtered Au nanoparticles was extremely weak in comparison with standard, commercial α-, and β-nucleants.[13]

In this contribution, we focused our attention on elucidation of the above-mentioned conflicting results by means of an improved sandwich method. We compared the nucleating activity of a strong nucleating agent (commercial α-nucleant Hyperform HPN-68) with the nucleating activity of gold microcrystals and nanocrystals with various morphologies, including chemically synthesized gold microcrystals with well-developed crystal facets[14] and vacuum-sputtered gold nanoparticles, nanoislands, and nanolayers. The sandwich method includes two steps: (i) preparation of sandwich nanocomposites and (ii) evaluation of nucleating activity in the sandwich nanocomposites. Briefly, the preparation of sandwich nanocomposites consists in controlled deposition of nucleant layer between thin PP films; the main improvement of the method lied in more reproducible preparation of sandwich specimens as described below. The evaluation of nucleating activity in the sandwich nanocomposites is carried out by three independent techniques: polarized-light microscopy (PLM), two-dimensional wide-angle X-ray scattering (2D-WAXS), and differential scanning calorimetry (DSC). The combination of carefully controlled sample preparation with the final evaluation of nucleating activity by the three completely different techniques (microscopy, diffraction, and thermal experiments) makes the method very sensitive and the results quite reliable and reproducible.

EXPERIMENTAL

Materials

Isotactic polypropylene Mosten GB 005 (iPP; general-purpose homopolymer, Unipetrol, Czech Republic) was used for preparation of sandwiches. Commercially available α-nucleating agent Hyperform HPN-68 (mixture of organic compounds and silicon dioxide; Milliken Chemical) was used for control experiments. Gold nanoparticles (AuNP; size = 5 nm), gold nanoislands (AuNI; size = 30 nm), and gold nanolayer (AuNL; continuous layer of gold nanocrystals ~ 15 nm thick) were prepared in a vacuum sputter coater EM SCD 050 (Leica). Gold microcrystals [AuMC; with well developed crystal facets, predominantly (111); size in micrometer scale] were prepared as described in our previous work.[14]

Preparation of sandwich nanocomposites

Preparation of sandwich nanocomposites consists of three steps: (i) careful preparation of clean PP films with selected thickness in the range 50–300 μm, (ii) homogeneous dispersion of micro nucleating/nanonucleating agent on the surface of PP film, (iii) thermal treatment of the prepared sandwiches, that is, PP films with nucleant layer(s), before/during PLM, DSC, and 2D-WAXS.

The clean PP films for sandwich composites were prepared as follows: PP granules were melt-mixed (Brabender Plasti-Corder PLE 651; 190°C, 10 min, and 60 rpm) and compression molded to 4 mm thick plates in a hot press (hydraulic press Fontijne Holand; 200°C for 4 min). The 50 μm PP films were prepared from the rectangular specimens cut from the molded PP plates (4 mm × 4 mm × 160 μm; the 160 μm thickness obtained with a sledge microtome). The samples were slightly compressed between two microscopic support glasses (both the samples and the glasses were carefully cleaned with a commercial detergent and washed with distilled water) at elevated temperature (Kofler bench at 220°C, 2 min, and load 1.5 kg; two 50 μm aluminum foils placed between the glasses to set required thickness; the glasses and the aluminum foils were preheated in an oven at 225°C). At the end, the sample was left to equilibrate at ambient temperature (>15 min, still between the glasses, load 0.75 kg). The 100/300 μm samples was obtained in the same way, only the initial thickness of the specimens was 400/1200 μm and the thickness of the aluminum foils was during the compression was 100/300 μm.

The homogeneous dispersion of nucleating agents on PP-films is illustrated in Figure 1. For each type of nucleant, slightly different strategy was used to achieve maximal homogeneity. Microcrystalline commercial α-nucleating agent [α; Fig. 1(b)] was dispersed in acetone (60 mg in 4 mL) and 5 μL of the dispersion was dropped onto a PP film (round film, $d = 6$ mm) and left to evaporate at ambient temperature. Ethanol suspension of gold microcrystals [~ 0.2 g of AuMC in 3.4 mL; Fig. 1(c)] was vigorously shaken and 5 μL of the suspension was directly dropped onto a PP film and left to evaporate. Vacuum sputtered gold nanoparticles [AuNP; Fig. 1(d)], gold nanoislands [AuNI; Fig. 1(e)], and gold nanolayer [AuNL; Fig. 1(f)] were directly sputtered onto the surface of a PP film. It should be noted that the AuNP, AuNI, and AuNL were sputtered both on PP films (for sandwich preparation) and on an electron-transparent carbon film [for more precise and convenient characterization by electron microscopy; Figs. 1(d–f)].

The final preparation of sandwich systems for PLM, DSC, and 2D-WAXS experiments is summarized

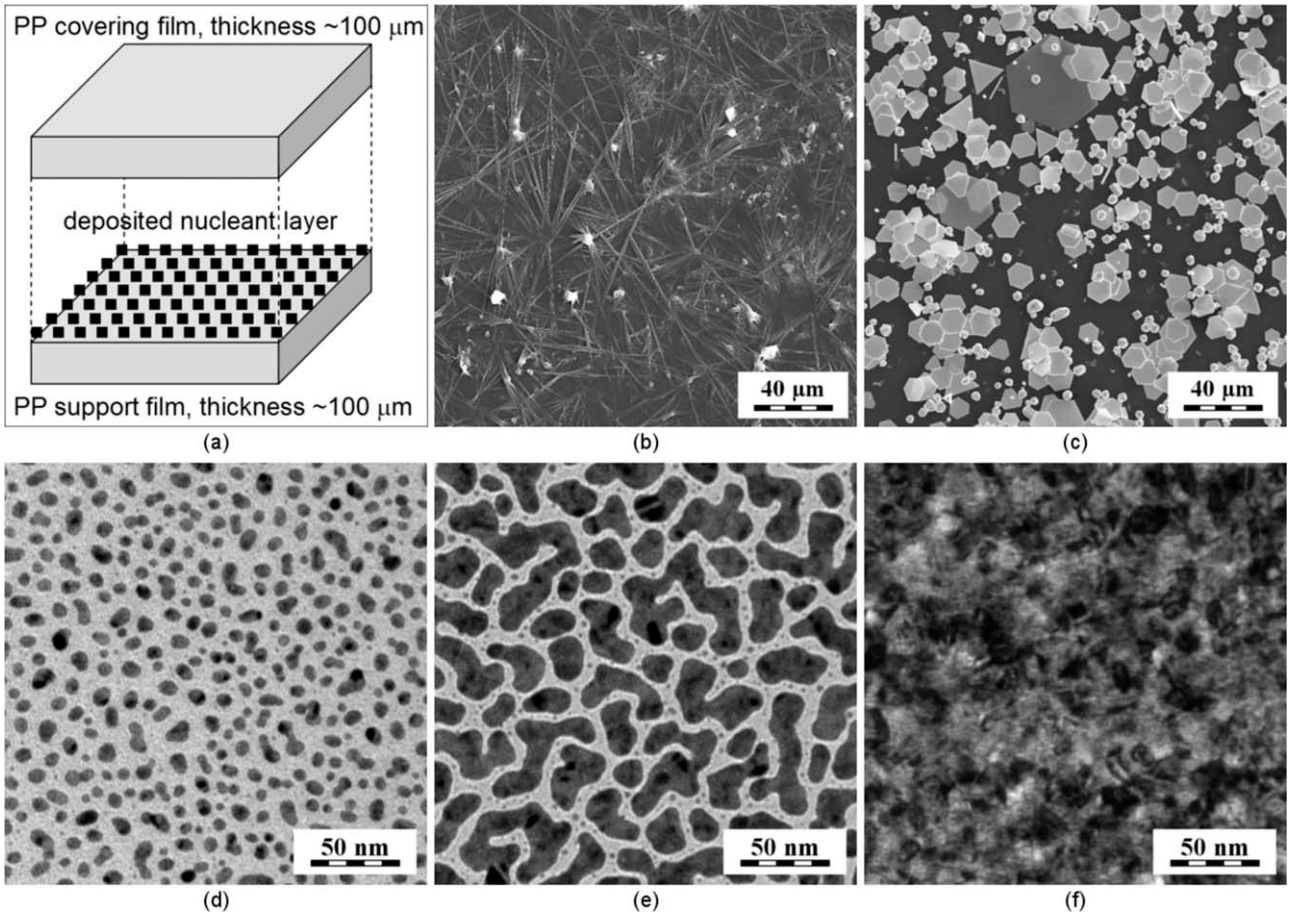

Figure 1 Preparation of nucleant nanolayer in sandwich samples: (a) schematic preparation of single sandwich; (b,c) SEM micrographs showing homogeneous dispersion of micronucleants on PP films: (b) α-nucleating agent and (c) gold microcrystals, AuMC; (d–f) TEM micrographs showing (d) gold nanoparticles, AuNP, (e) gold nanoislands, AuNI, and (f) gold nanolayer, AuNL, which were vacuum-sputtered on a carbon film.

schematically in Figure 2. PLM sandwiches [Fig. 2(a)] were prepared from two 100 μm films. The round films ($d = 6$ mm) with 0 or 1 nucleant layer were heated in a hot bar (Kofler bench, 200°C for 8 min and then 120°C for 30 min) and left to equilibrate at room temperature. Cross-sections (thickness 5 micrometers) were cut at laboratory temperature with a glass knife using an ultramicrotome Ultratome III (LKB). DSC sandwiches [Fig. 2(b)] were prepared from four 50 μm films: The round films ($d = 6$ mm) were covered with 0, 1, 2, or 3 layers of the nucleant and closed in the DSC aluminum pans. 2D-WAXS sandwiches [Fig. 2(c)] were prepared in exactly the same way as PLM sandwiches, only the thickness of PP films was 300 μm and the final cross-sections of the sandwiches was 2 mm thick.

Evaluation of nucleating activity in sandwich nanocomposites

As mentioned above, the nucleation effects in sandwich nanocomposites were observed by three independent methods (PLM, DSC, and 2D-WAXS). As for PLM, the cross-section of a sandwich [Fig. 2(a)] was observed in transmitted polarized light in a microscope Zetopan Pol (Reichert). PLM micrographs were recorded with a digital camera DXM 1200 (Nikon).

As for DSC, a multilayered sandwich [Fig. 2(b)] in the aluminum pan was transferred to a calorimeter PYRIS 1 DSC (Perkin-Elmer). A sample was heated three times from 30 to 220°C at heating rate 120°C/min, annealed at this temperature for 8 min, and after that cooled to 30°C at cooling rate 10°C/min. DSC curves were processed with the standard calorimeter software and the crystallization temperature (T_C; minimum on the crystallization exotherm) and the onset crystallization temperatures (T_O; intersection of the baseline and inflection line of the crystallization peak) were determined and averaged. Moreover, for each type of sandwich we prepared at least three samples. Last but not the least, the measurements were performed in inert atmosphere and the apparatus was regularly calibrated, using an indium standard, to achieve maximum reliability and reproducibility.

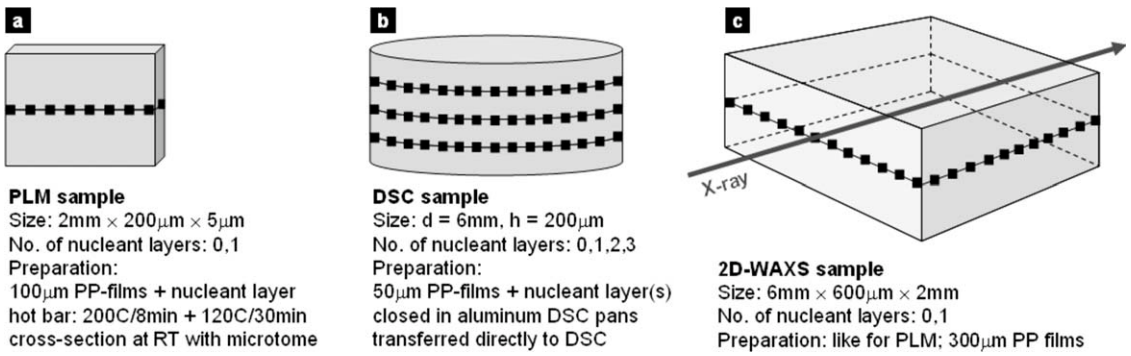

Figure 2 Preparation of sandwich nanocomposites for PLM, DSC, and 2D-WAXS; PP films are gray, nucleant particles are represented by small black squares.

As for 2D-WAXS, the cross-section of the sandwich was probed with an X-ray beam going through the centre of the sample, along the nucleant layer [Fig. 2(c)]. Before each measurement, the X-ray beam (diameter of the beam 300 μm) was centered in the middle of the sample by a fast absorption scan. Wide-angle X-ray diffraction patterns of all samples were recorded using a system with a pinhole camera (Molecular Metrology SWAXS System) attached to a microfocused X-ray beam generator (Osmic MicroMax 002) operating at 45 kV and 0.66 mA (30 W). The diffraction patterns of the sandwich samples were recorded with a two-dimensional image plate detector. Azimuthal scans, showing the intensity of the strongest diffraction of α-spherulites (110) in various positions on the detector (0–360°; step 1°), were calculated using our own script in MATLAB language (MathWorks). Each sample was measured at least three times and the final azimuthal scans were further processed as described below.

Processing and statistical evaluation of the results

PLM micrographs were evaluated only on qualitative level. Azimuthal scans from 2D-WAXS diffraction patterns were processed with a standard spreadsheet program Excel (Microsoft). In the first step, the azimuthal scans were normalized, smoothed, and averaged. In the second step, the sums of square deviations of the processed azimuthal scans from the hypothetical, ideally isotropic sample were calculated. Crystallization and onset temperatures from DSC (T_C's and T_O's) were also processed in Excel: arithmetic means, standard deviations, and unpaired, unequal variance two-sample *t*-tests at 95% confidence level were calculated using standard functions of the program. Final 2D-WAXS and DSC results were plotted using a freeware program gnuplot (www.gnuplot.info).

RESULTS

Polarized light microscopy

PLM micrographs of thin cross-sections through the sandwich samples show the nucleated crystallization in real/direct space (Fig. 3). The sandwiches for PLM microscopy consist of two 100 μm PP films with 0 or 1 layer of the nucleant between the films [Fig. 2(a)]. We studied six types of these sandwich nanocomposites by PLM: a sandwich with no nucleating agent (the first control sample, denoted as PP/0), a sandwich with commercial α-nucleating agent [the second control sample, denoted as PP/α; nucleant layer in Fig. 2(b)], and a four sandwich samples with gold nanolayers, which were formed by gold microcrystals [PP/AuMC; Fig. 2(c)] nanoparticles [PP/AuNP; Fig. 2(d)], nanoislands [PP/AuNI; Fig. 2(e)], and nanolayer [PP/AuNL; Fig. 2(f)].

PLM micrograph of the sandwich without nucleating agent, PP/0, displayed randomly growing spherulites [Fig. 3(a)]. In contrast, the sandwich with commercial α-nucleating agent, PP/α, exhibited strong oriented crystallization starting from the central nucleant layer [Fig. 3(b)]; such a strong nucleation from a line or a layer is frequently called transcrystallization.[15] Sandwich with gold microcrystals, PP/AuMC [Fig. 3(c)], also showed transcrystallization; although, it was evidently less intensive than in the case of PP/α. Sandwiches with vacuum-sputtered gold nanoparticles [Fig. 3(d)], nanoislands [Fig. 3(e)], and nanolayer [Fig. 3(f)] indicated only very weak nucleating activity: just a few spherulites grew from the nucleant layer. According to the PLM micrographs, the difference between the three sandwiches with vacuum-sputtered gold (PP/AuNP, PP/AuNI, and PP/AuNL) and the control sample without nucleant (PP/0) was almost negligible.

2D wide-angle X-ray scattering

2D-WAXS diffractograms of thick cross-sections through the sandwich samples show the nucleated-crystallization-induced orientation in diffraction/reciprocal space (Fig. 4). The sandwiches for 2D-WAXS consisted of two 300 μm films with 0 or 1 layer of the nucleant between them [Fig. 2(c)]. The increased thickness of sandwiches for 2D-WAXS (∼ 600 μm) in comparison with the sandwiches for

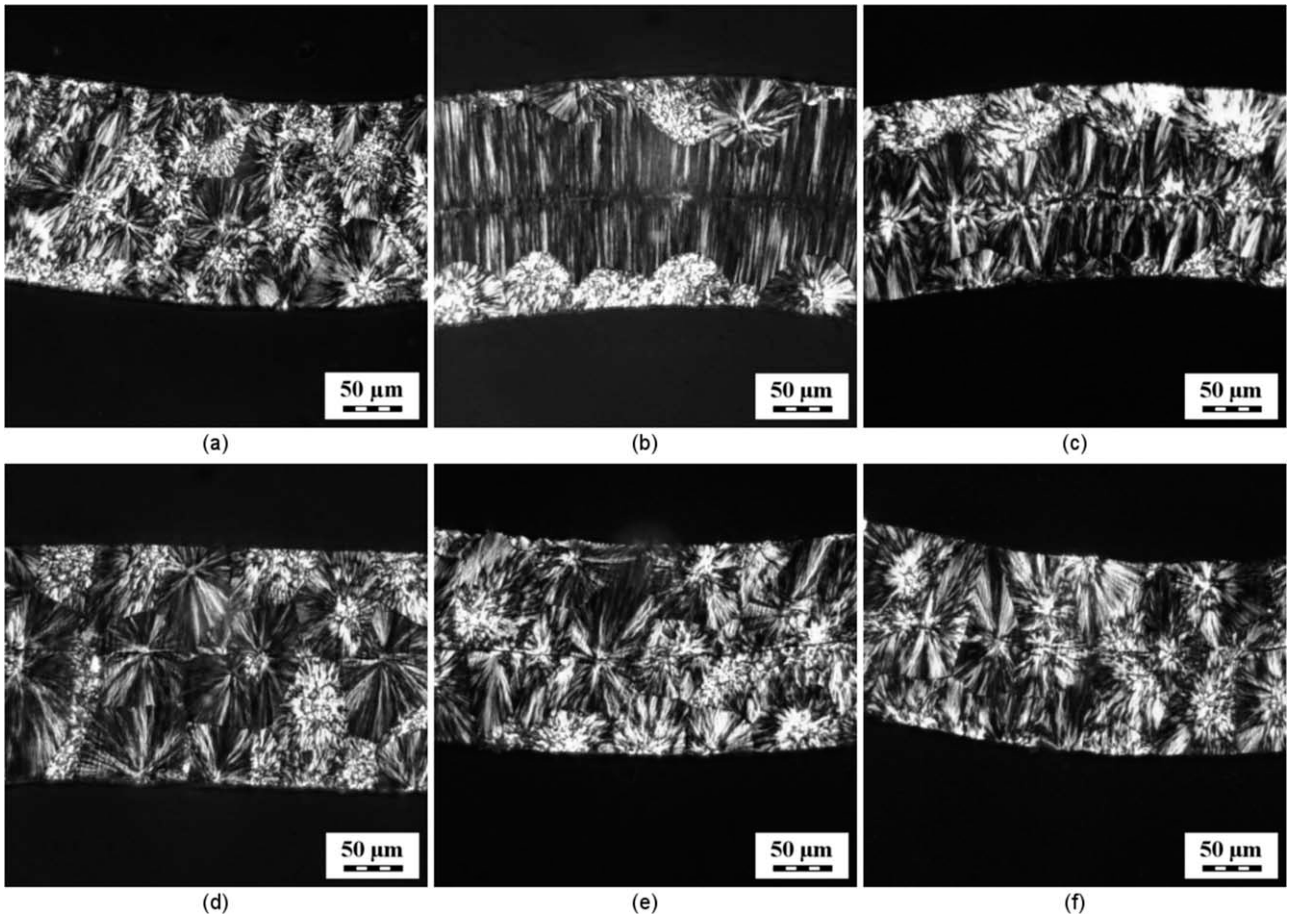

Figure 3 Sandwich method, representative PLM micrographs showing cross-sections of sandwich structures with spherulites that grow from nucleant layers: (a) PP/0, (b) PP/α, (c) PP/AuMC, (d) PP/AuNP, (e) PP/AuNI, and (f) PP/AuNL.

PLM (~ 200 μm) was necessary because the X-ray beam diameter in our diffractometer had a nonzero diameter (~ 300 μm). Consequently, 2D-WAXS diffractograms of 200 μm sandwiches would have been influenced by the surface nucleation from both edges of the PP films, which was observed both here in PLM micrographs (Fig. 3) and in a number of previous studies (e.g., Refs. 13 and 16). In the time-consuming 2D-WAXS experiments, we studied five sandwiches (PP/0, PP/AuNP, PP/AuNL, PP/AuMC, and PP/α); the sandwich PP/AuNI was excluded, because it was almost identical with PP/AuNP and PP/AuNL according to PLM results.

2D-WAXS results in the form of azimuthal scans are summarized in Figure 4. The inset in Figure 4 shows the definition of the azimuthal angle for an indexed diffraction pattern of PP/α sandwich, which exhibited the strongest orientation due to nucleated crystallization. Detailed explanation of the relationship between the orientation of the lamellae in the real/direct space and azimuthal angle in the diffraction/reciprocal space was given in our previous study,[13] in which we used somewhat different sandwiches, but geometry of the diffraction experiments was exactly the same. In Figure 4, the thin solid line denotes hypothetical, ideally isotropic sample. Sample with commercial α-nucleating agent, PP/α,

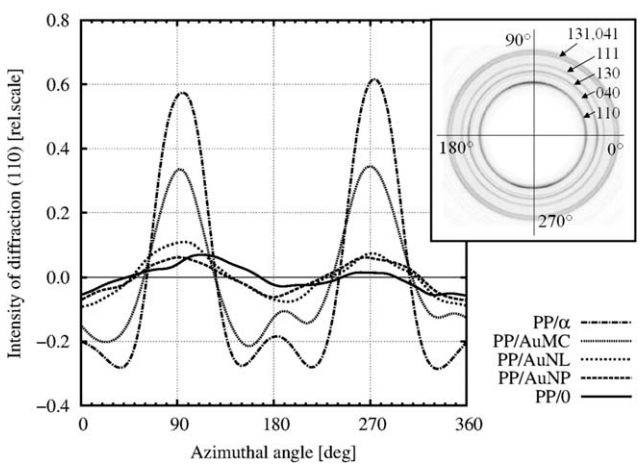

Figure 4 Sandwich method, 2D-WAXS results. Graph shows azimuthal scans along the strongest PP diffraction (110); thin full line denotes ideally isotropic sample. Inset shows indexed 2D-WAXS diffraction pattern of PP/α sandwich with definition of azimuthal angle.

TABLE I
2D-WAXS Results: Normalized Sums of Square Deviations from Ideally Isotropic Sample

Sample	μ	σ	*n*
PP/0	1.4	1.0	3
PP/AuNC	2.4	1.6	6
PP/AuNL	3.9	2.1	3
PP/AuMC	35.9	24.8	3
PP/α	100.0	51.5	4

The average values (μ) represent normalized sum of square deviations from the azimuthal scan of diffraction (110) in an ideally isotropic PP sample, which would have $\mu = 0$. The normalization was performed in such a way that the sample with maximum anisotropy (PP/α) was assigned $\mu = 100$. The estimated standard deviations (σ) and number of independent measurements (*n*) illustrate the scatter of the data.

showed the strongest deviation from this ideally isotropic case. Sandwich with gold microcrystals, PP/AuMC, also exhibited quite strong orientation, although it was lower in comparison with PP/α. Nucleation in sandwich composites with vacuum-sputtered gold, PP/AuNP, and PP/AuNL, was substantially lower. All 2D-WAXS results were in very good agreement with the nucleated crystallization observed directly in PLM micrographs (cf. Figs. 3 and 4).

Control sample without nucleating agent, PP/0, which should have been ideally isotropic according to both general considerations and PLM results, exhibited very small, but non-negligible anisotropy in 2D-WAXS. This was attributed to residues of surface nucleation between PP films, which was observed also in our previous studies[12,13]; although, we did our best to eliminate the surface nucleation by thermal treatment. The results suggested that the surface nucleation between PP films was rare and, as a result, it was not observed in the thin 5 μm cross-sections for PLM [Fig. 3(a)], but the small residues of the nucleation were detectable in substantially thicker, 2 mm cross-sections for 2D-WAXS (Fig. 4).

Quantitative evaluation of 2D-WAXS results is summarized in Table I. Azimuthal scan of each sample was characterized by a normalized sum of square deviations (NSSD) from an ideally isotropic sample. The normalization was performed in such a way that the hypothetical, ideally isotropic sample would have had NSSD = 0, whereas the sample with strongest orientation due to nucleated crystallization, PP/α, was set to NSSD = 100. The quantitative results confirmed that the nucleating activity decreased in the following order: PP/α > PP/AuMC > PP/AuNL ≥ PP/AuNP ≥ PP/0. The estimated standard deviations suggested that there were considerable differences between several samples with the same nucleants. Parallel microscopic and diffraction experiments showed that the differences existed even within each sample, because the originally compact and homogeneous nucleant layer was partially torn into 2D-pieces after the thermal treatment and, consequently, the results depends on the particular position of the X-ray beam. As a result, the relatively large estimated standard deviations in 2D-WAXS are not critical and can be eliminated in the future experiments if each sample is measured in several locations. Moreover, it is possible to conclude that the final agreement between qualitative evaluation of PLM micrographs and quantitative evaluation 2D-WAXS azimuthal scans was very good.

Differential scanning calorimetry

DSC experiments were focused on three problems: (i) check of the reproducibility of the method by means of multiple-layered sandwiches, (ii) verification of PLM and 2D-WAXS results by yet another independent method, and (iii) finding a difference among PP/0, PP/AuNP, and PP/AuNL, which seemed to be almost the same according to PLM and 2D-WAXS results. In DSC, the nucleated PP crystallization demonstrates itself by increase in crystallization temperature (T_C) and onset crystallization temperature (T_O), which were defined in the experimental section above. Sandwich samples for DSC experiments were only 50 μm thick [to maximize nucleant/PP ratio; Fig. 2(b)] and had several nucleant layers (to check that the T_C and T_O increase reproducibly with the number of layers, that is, with the increasing concentration of the nucleating agent).

The applicability of DSC on sandwich specimens was checked in multiple-layered PP/α sandwich nanocomposites with 0, 1, 2, and 3 layers of nucleant (Fig. 5). For each number of layers, three independent samples were measured in DSC and the shifts of both T_C and T_O could be observed clearly after averaging the results. Both ΔT_C and ΔT_O grew reproducibly with the increasing number of nucleant layers. Although the absolute values of ΔT_C ($\sim 2^\circ$C) and ΔT_O ($\sim 5^\circ$C) were not too big, the difference between the sample with zero and three layers of nucleant were statistically significant as indicated by estimated standard deviations in Figure 5 and evidenced by two-sample *t*-tests ($P = 0.0168$ for ΔT_C; $P = 0.0001$ for ΔT_O).

The DSC results for PP/0, PP/AuNP, and PP/AuNL sandwich nanocomposites are summarized in Figure 6. In the first step, we checked the increase in T_C and T_O for multiple-layered PP/AuNP sandwiches with 0, 1, 2, and 3 nucleant layers [Fig. 6(a,b)]. As expected, the T_C and T_O shifts were smaller than in the case of analogous PP/α series

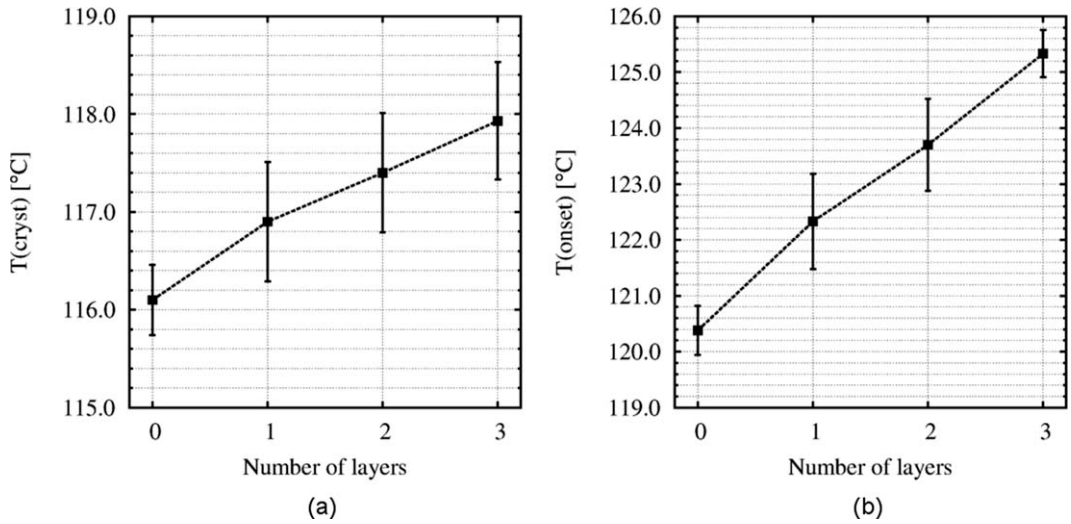

Figure 5 Sandwich method, DSC results, part 1: (a) Crystallization and (b) onset temperatures for PP/α sandwich structures with 0–3 layers of commercial α-nucleant. Error bars represent estimated standard deviations.

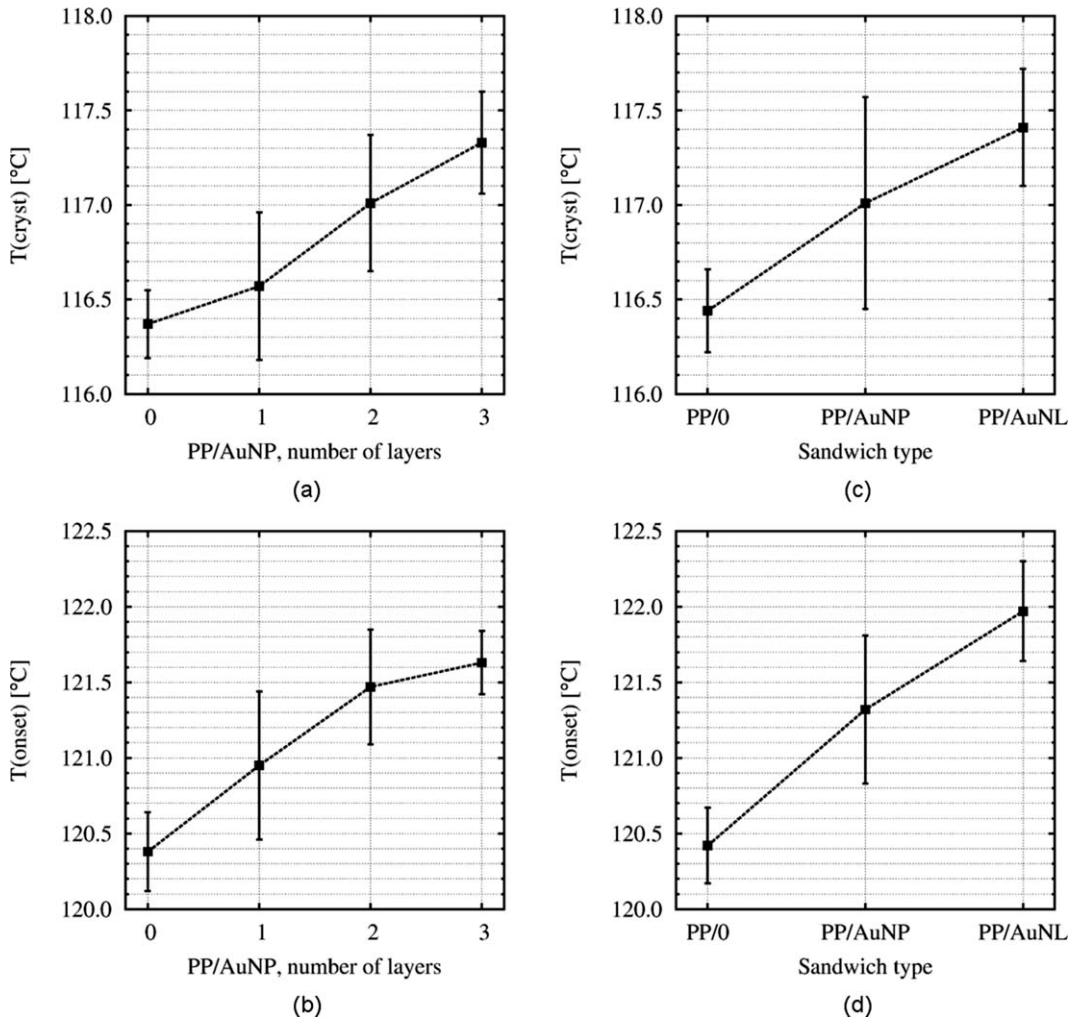

Figure 6 Sandwich method, DSC results, part 2: (a) Crystallization and (b) onset temperatures for PP/AuNP sandwich structures with 0–3 layers of vacuum-sputtered Au nanoparticles; (c) crystallization and (d) onset temperatures for PP/0, PP/AuNP, and PP/AuNL sandwiches with three layers of nucleant. Error bars represent estimated standard deviations.

TABLE II
DSC Results: Basic Statistical Evaluation of T_C and T_O for Three-Layered Sandwiches PP/0, PP/AuNP, and PP/AuNL

		T_C (°C)		T_O (°C)	
Sample	n	μ	σ	μ	σ
PP/0	5	116.4	0.2	120.4	0.3
PP/AuNP	6	117.0	0.6	121.3	0.5
PP/AuNL	7	117.4	0.3	122.0	0.4

The values of n, μ, and σ are number of samples/measurements, arithmetic mean, and estimated standard deviation, respectively.

(Fig. 5). Nevertheless, the difference between PP/0 and PP/AuNP with three nucleant layers were statistically significant as well ($P = 0.0018$ for ΔT_C; $P = 0.0003$ for ΔT_O) on condition that sufficient number of experiments (in this case, four measurements per sample) was performed. In the second step, we prepared completely new sandwich samples for new set of experiments, whose objective was to verify the method reproducibility and to check the difference between PP/AuNP and PP/AuNL sandwich nanocomposites with three layers of nucleant [Fig. 6(c,d)]. Statistical evaluation of the results is given in Tables II and III. In general, the agreement between the corresponding samples (PP/0 and PP/AuNP with three nucleant layers) in the first set of experiments [Fig. 6(a,b)] and the second set of experiments [Fig. 6(c,d)] was acceptable, although the scatter of the data, represented by estimated standard deviations, was quite high. The observed shifts in T_C [Fig. 6(c)] were less intensive than the shifts in T_O, which was in agreement with the results for PP/α sandwiches (Fig. 5). Accordingly, the slightly higher nucleating activity of PP/AuNL in comparison with PP/AuNP was more statistically significant in case of ΔT_O (Table III).

It has been demonstrated that during the crystallization of thin PP films in DSC, there was some nucleation activity from the surface of DSC aluminum pans.[16] This effect was further verified and modeled by means of theoretical calculations.[17] Nevertheless, in our case of sandwich method the effect of aluminum pans was cancelled out, because the ΔT_C and ΔT_O shifts were always related to the control PP/0 specimen, which was measured under the same conditions including the same type of pans.

In conclusion, it has been demonstrated that DSC is applicable on sandwich specimens as a third, independent method. First, DSC results showed that the nucleating effect increased reproducibly with the increasing number of nucleant layers for both strong, commercial α-nucleating agent and weakly nucleating vacuum-sputtered gold nanoparticles. Second, the DSC results indicated that for weakly nucleating agents such as vacuum-sputtered gold, sufficient number of measurements (at least five per sample; see Table II) and sufficient number of nucleant layers (at least three in the sample; see Fig. 6) was necessary to achieve statistically significant results. Third, the DSC results were in quite good agreement with PLM and 2D-WAXS experiments and confirmed that the nucleating activity decreased in the row: PP/α > PP/AuMC > PP/AuNL ≥ PP/AuNP ≥ PP/0, where the symbol ≥ means that the difference was at the edge of experimental errors.

DISCUSSION AND CONCLUSION

The improved sandwich method, which is suitable for quantification of both very strong and extremely weak nucleating activity in iPP, was introduced in this work. The sandwich method has several advantages. First, the controlled deposition of nucleant layer onto the surface of PP films enables us to eliminate problems with agglomeration, which occur during melt mixing in bulk. Second, the sandwich specimens are quite small and so the method is suitable for testing specific nucleants, whose synthesis is not simple and their amount is limited, such as gold microcrystals in this work. Third, the sandwich method includes three independent techniques for evaluation of the results: (i) a local microscopic technique—polarized light microscopy—visualizes the nucleation activity directly; (ii) a semi-local diffraction technique—2D wide-angle X-ray scattering—evaluates the nucleation-induced orientation in reciprocal space; (iii) a thermal technique—differential scanning calorimetry—measures nucleation-induced shifts in crystallization and onset temperatures. The combination of the three mutually different and independent techniques makes the results more reliable.

This study was focused on nucleating activity of gold microparticles and nanoparticles with various

TABLE III
DSC Results: Statistical Comparison of T_C and T_O Values Obtained for Three-Layered Sandwiches PP/0, PP/AuNP, and PP/AuNL

Sample	PP/0	PP/AuNP	PP/AuNL
PP/0	1.000	0.005	0.000
PP/AuNP	0.058	1.000	0.027
PP/AuNL	0.000	0.145	1.000

The values in the table are P-values obtained from two-sample t-tests (unpaired, unequal variance t-test, 95% level of significance); values of P below 0.05 indicate statistically significant difference. Lower left triangle of the square table shows P-values for measured T_C's, upper right triangle shows P-values for measured T_O's. All P-values were calculated from the data summarized in Table II.

morphologies. In our previous work we found that melt-mixing of PP with a colloidal solution of chemically synthesized 5 nm gold nanocrystals resulted in quite intensive nucleation of PP crystallization.[12] In a parallel set of experiments, we investigated nucleated crystallization of PP by 5 nm vacuum-sputtered gold nanocrystals using the first version of the sandwich method and came to conclusion that the nucleating activity of the nanoparticles was extremely weak; the difference might have been attributed to different preparation of composites, slightly different morphology of chemically synthesized Au nanoparticles and/or certain Au surface contamination during chemical syntheses.[13] To elucidate these contradictory results, we applied the improved sandwich method (Figs. 1 and 2) to chemically synthesized gold microcrystals (AuMC), vacuum-sputtered gold nanoparticles (AuNP), nanoislands (AuNI) and nanolayers (AuNL). Combination of PLM, 2D-WAXS, and DSC results (Figs. 3–6) enabled us to order the nucleants according their nucleating activity as follows: PP/α > PP/AuMC > PP/AuNL $\geq$ PP/AuNP $\geq$ PP/0, where PP/α and PP/0 denote control sample with commercial α-nucleating agent and blank sample without any nucleant as described above. Provided that the nucleation activity of gold particles depended only on the size of the nucleant, the highest activity must have been observed for PP/AuNL sandwich nanocomposites. However, the nucleated crystallization in PP/AuMC was much higher than in the sandwiches with vacuum-sputtered gold, represented by PP/AuNP, PP/AuNI, and PP/AuNL.

All the above described experiments and results brought us to the following conclusions: (i) nucleating activity of Au in PP strongly depends on the morphology of gold particles, (ii) gold microcrystals with well developed (111) facets nucleate PP crystallization much more than vacuum-sputtered nanocrystalline gold, regardless of its size, as even the compact vacuum-sputtered gold nanolayer exhibited negligible nucleation activity, (iii) this probably explains why we had observed quite strong nucleation activity with 5 nm chemically synthesized gold nanocrystals,[12] whereas the nucleating activity on 5 nm vacuum-sputtered gold nanoparticles was found extremely weak[13] and, finally (iv) the strong impact of microcrystal and nanocrystal morphology on the nucleating activity, which has been demonstrated here, might explain also other contradictory results concerning nanonucleated crystallization of semicrystalline polymers in the literature.

The authors thank Mrs. Dagmar Ondruskova and Miss Hana Sandova for DSC and 2D-WAXS measurements, respectively.

References

1. Gross S. In Handbook of plastic materials and technology; Rubin, I. I., Ed.; Wiley-Interscience: New York, 1990; Chapter 1.
2. Hanna, R. D. In Handbook of plastic materials and technology; Rubin I. I., Ed.; Wiley-Interscience: New York, 1990; Chapter 38.
3. Mathieu, C.; Thierry, A.; Wittmann, J. C.; Lotz, B. Polymer 2000, 41, 7241.
4. Mathieu, C.; Thierry, A.; Wittmann, J. C.; Lotz, B. J Polym Sci Part B: Polym Phys 2002, 40, 2504.
5. Varga, J.; Ehrenstein, G. W. In Polypropylene: An A-Z reference; Karger-Kocsis, J., Ed.; Kluwer Academic Publishers: London, 1999; Chapter: Beta-modification of isotactic polypropylene.
6. Gedde, U. V. Polymer Physics; Chapman and Hall: London, 1995.
7. Pawlak, A.; Morawiec, J.; Piorkowska, E.; Galeski, A. Solid State Phenom 2003, 94, 335.
8. Qian, J.; He, P.; Nie, K.; He, P. J Appl Polym Sci 2004, 91, 1013.
9. Jain, S.; Goossens, H.; van Duin, M.; Lemstra, P. Polymer 2005, 46, 8805.
10. Tjong, S. C.; Bao, S. e-Polymers 2007; available at: http://www.e-polymers.org.
11. Slouf, M.; Kuzel, R.; Matej, Z. Z. Kristallogr. Suppl. 23, 2006, 319.
12. Masirek, R.; Szkudlarek, E.; Piorkowska, E.; Slouf, M.; Kratochvil, J.; Baldrian, J. J Polym Sci Part B: Polym Phys 2010, 48, 469.
13. Pavlova, E.; Slouf, M.; Sandova, H.; Baldrian, J.; Sikora, A.; Lednicky, F.; Masirek, R.; Piorkowska, E. J Macromol Sci Part B: Polym Phys 2010, 49, 392.
14. Base, T.; Bastl, Z.; Slouf, M.; Klementova, M.; Subrt, J.; Vetushka, A.; Ledinsky, M.; Fejfar, A.; Machacek, J.; Carr M. J.; Londesborough G. S. J Phys Chem C 2008, 112, 14446.
15. Houshyar, S.; Shanks, R. A. e-Polymers 2010; available at: http://www.e-polymers.org.
16. Gadzinowska, K.; Piorkowska, E. Polimery 2003, 48, 790.
17. Piorkowska, E.; Billon, N.; Haudin, J. M.; Gadzinowska, K. J Appl Polym Sci 2005, 97 2319.